Bull. Mater. Sci., Vol. 39, No. 1, February 2016, pp. 307–313. © Indian Academy of Sciences.

Bias-dependent photo-detection of dual-ion beam sputtered MgZnO thin films

SAURABH KUMAR PANDEY* and **SHAIBAL MUKHERJEE**

Discipline of Electrical Engineering, Indian Institute of Technology, Indore 452003, India

MS received 23 July 2015; accepted 21 September 2015

Abstract. **The structural, morphological, elemental and electrical properties of MgZnO thin films, grown on p-Si (001) substrates by dual-ion beam sputtering deposition (DIBSD) system at different substrate temperatures were thoroughly investigated. X-ray diffraction (XRD) pattern of MgZnO film exhibited crystalline hexagonal wurtzite structure with the preferred (002) crystal orientation. The full-width at half-maximum of the (002) plane was the narrowest with a value of 0.226° from MgZnO film grown at 400°C. X-ray photoelectron spectroscopy analysis confirmed the substitution of Zn^{2+} by Mg^{2+} in MgZnO thin films and the absence of MgO phase. Correlation between calculated crystallite size, as evaluated from XRD measurements, and room-temperature carrier mobility, as obtained from Hall measurements, was established. Current–voltage characteristics of MgZnO thin films were carried out under the influence of dark and light illumination conditions and corresponding values of photosensitivity were calculated. MgZnO film grown at 100°C exhibited the highest photosensitivity of 1.62. Compared with one of the best-reported values of photosensitivity factor from ZnO-material-based films available in the literature, briefly, ∼3.085-fold improved photosensitivity factor at the same bias voltage (2 V) was obtained.**

Keywords. **DIBSD; growth temperature; Hall measurements; MgZnO thin films; XRD; XPS.**

1. Introduction

Ultraviolet (UV) photodectection have become subject of intense research because of various new requirements in technological fields, such as flame detection, engine monitoring, missile plume detection, chemical sensing and inter-satellite communications [1,2]. ZnO-based material systems have been promising for advanced electronic and opto-electronic devices because of the availability of wide direct band gap of 3.37 eV and large free exciton binding energy of 60 meV [3–9] at room temperature. MgZnO is an important semiconductor alloy for application to deep-UV photodetectors (PDs) and optoelectronic devices such as solar UV radiation monitors, ultrahigh temperature flame detectors, air-borne missile warning systems, space communication systems and ozone layer monitors [10,11]. Alloying ZnO films with MgO facilitates suitable band-gap engineering for device design. It has been reported that band gap energy increases considerably from 3.37 to 7.8 eV on varying the x-composition for ternary compound $Mg_xZn_{1-x}O$ from 0 to 1 [11,12]. The ionic radius of Mg^{2+} (0.57 Å) is similar to that of Zn^{2+} (0.6 Å), so replacement of Zn^{2+} by Mg^{2+} should not cause a significant change in lattice constants [13]. In order to improve internal quantum efficiency of light emitters, the application of MgZnO layers as electron and hole blocking layers is quite essential [14].

A number of deposition techniques have been deployed to grow MgZnO films such as pulsed-laser deposition [15], molecular beam epitaxy [16], metal-organic chemical vapour deposition [17,18] and radio frequency (RF) sputtering [19]. Among these deposition techniques, dual-ion beam sputtering deposition (DIBSD) technique is quite popular since it gives rise to high-quality and uniform film growth on larger substrate area at relatively lower substrate temperature [20,21]. Detailed descriptive analysis on the influence of growth temperature on the photoconducting properties of DIBSD-grown MgZnO has not been reported yet. Therefore, it will be extremely interesting to study the dependence of photoconduction of such MgZnO films in view of realizing high-performance optoelectronic and photovoltaic devices.

In this study, the effect of substrate temperature on the growth of ternary MgZnO films by DIBSD system has been discussed and characterizations of such films were performed to determine and correlate structural, elemental, morphological and electrical properties of thin MgZnO films. Current–voltage (I–V) characteristics of the MgZnO thin films were carried out in dark and under UV-illumination under different bias conditions.

2. Experimental

DIBSD system [22,23] was used to deposit MgZnO thin films of thickness ∼600 nm in the base pressure of 3×10^{-4} mbar on p-Si (001) substrates. During the growth process, a

*Author for correspondence (saurabh.rjit@gmail.com)

secondary direct-current assist ion source with the primary RF ion source was deployed to increase the film adhesion to the substrate and to eventually realize more uniform film surface. Before inserting into DIBSD growth chamber, Si substrates were rinsed thoroughly with trichloro-ethylene, acetone, iso-propanol and de-ionized (DI) water and then purged by high-purity (99.999%) N_2 gas. Film growth was accomplished by sputtering a water-cooled, 4-in-diameter $Mg_{0.1}Zn_{0.9}O$ target (99.99%) at various substrate temperatures, ranging from 100 to 600°C. During the reactive sputtering process, the flow rate ratio of oxygen (99.999%) and argon gases (99.999%) was maintained at 4 : 2 where primary ion beam power was kept constant at 65 W.

The structural properties of MgZnO films were examined by X-ray diffraction (XRD) using a Bruker D8 Advance X-ray diffractometer with a Cu-K_α radiation ($\lambda = 0.154$ nm). X-rays, produced inside a sealed tube, were detected after getting diffracted from the sample surface using a fast counting detector based on the silicon strip technology (Bruker Lynx Eye detector). Surface morphology and roughness of

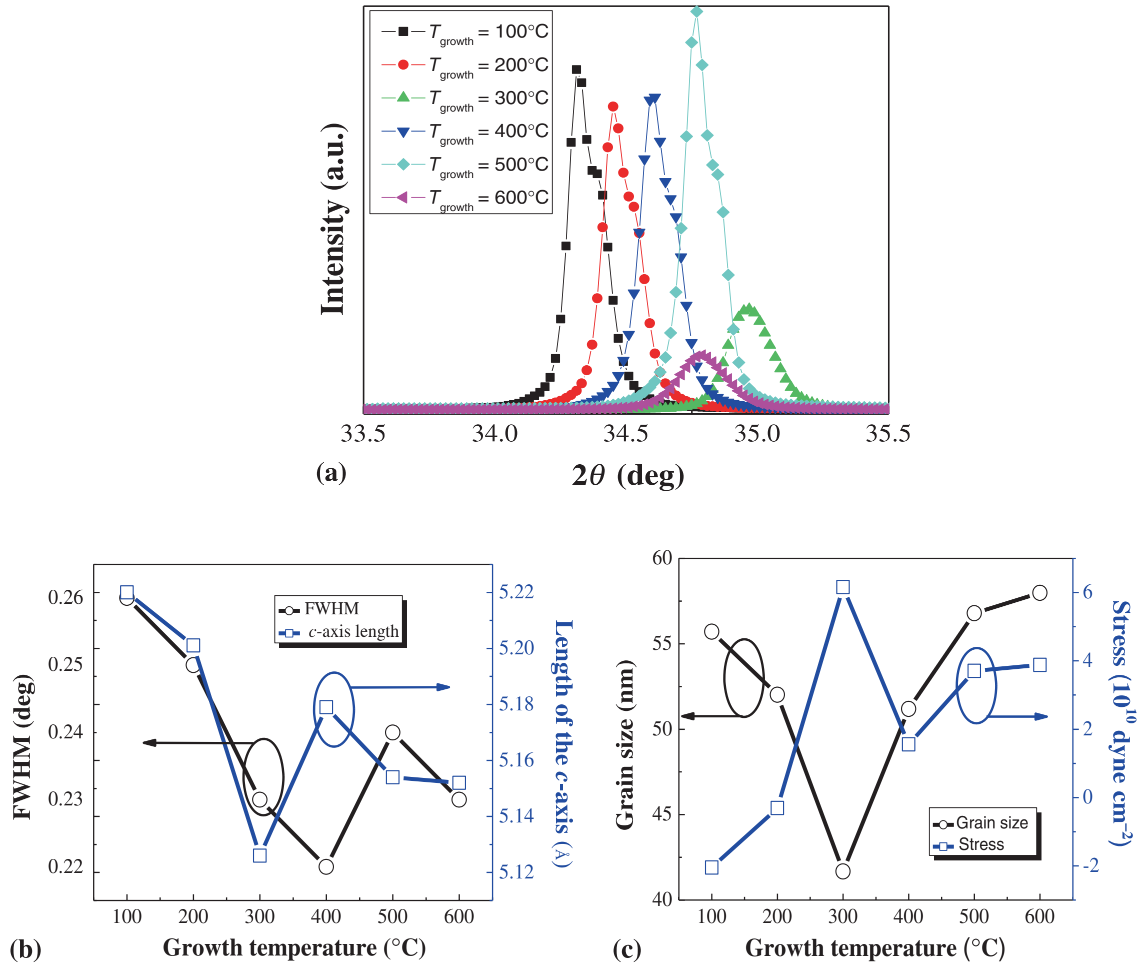

Figure 1. (**a**) XRD patterns of MgZnO (002) peaks, (**b**) FWHM and the *c*-axis length of MgZnO (002) peaks and (**c**) crystallite size and stress generation on MgZnO thin films for different growth temperatures.

Table 1. Influence of growth temperature on stress and crystallite size of MgZnO thin films grown on p-Si (001) substrate.

Growth temp. (°C)	(002) peak value	FWHM (deg)	Lattice constant, c (Å)	Crystallite size (nm)	Stress ($\times 10^{10}$ dyne cm^{-2})
100	34.313	0.149	5.220	55.707	−2.049
200	34.450	0.160	5.201	52.011	−0.306
300	34.968	0.200	5.126	41.669	+6.159
400	34.597	0.163	5.179	51.180	+1.554
500	34.769	0.147	5.154	56.790	+3.707
600	34.786	0.144	5.152	57.977	+3.879

deposited films were measured by using advance integrated scanning tools for nano-technology (AIST-NT), atomic force microscope (AFM) and ZEISS Supra55 field-emission scanning electron microscope (FE-SEM). I–V characteristics of the MgZnO thin films were measured by using 325 nm He–Cd (10 mW) laser and Keithley 2612A source meter.

X-ray photoelectron spectroscopy (XPS) measurement was performed on MgZnO film grown at 300°C to validate the presence of elemental Mg in MgZnO using a PHOIBOS 100 analyzer with an Al-K_{α} radiation (1486.6 eV) as an excitation source. The sample surface was pre-etched using 1 keV Ar ion beam before performing XPS measurement to remove air contaminated top layer. Various chemical species were identified from their corresponding binding energies. The binding energies were determined by fitting the XPS spectral line shapes with Lorentzian–Gaussian functions. The room-temperature sheet-resistivity, carrier concentration and mobility of MgZnO thin films were measured by four-probe Hall-effect measurements in the van der Pauw configuration using 2612A Keithley source meter and a magnetic field of ∼0.5 T.

3. Results and discussion

Figure 1a depicts the XRD pattern of MgZnO thin films grown on the p-Si (001) substrate as a function of substrate temperature. The $[\omega - 2\theta]$ XRD pattern clearly reveals that MgZnO thin films grown is highly c-axis oriented hexagonal wurtzite structures with preferred (002) crystal orientation as reported in existing literatures. It was observed from table 1 that the position of the (002) diffraction peak shifted from 34.313° at 100°C to 34.968° at 300°C and then became irregular and finally reached to 34.786° for the film deposited at 600°C. It is well known that the angular peak position of $Mg_{0.1}Zn_{0.9}O$ powder is located at 34.473° [24].

The shift in the corresponding diffraction peak position for different growth temperatures was mainly due to strain produced within the films during growth process. The angular peak position of film grown at 100°C, as observed in figure 1a, is less than the angular value of $Mg_{0.1}Zn_{0.9}O$ powder peak; indicating that the lattice constant (c) of the MgZnO films was elongated as compared with the MgZnO single crystal and the unit cells are under compressive stress. It was also observed that with an increase in growth temperature, the c-axis plane peak position shifted towards the angular value of $Mg_{0.1}Zn_{0.9}O$ powder peak. The peak position becomes 34.450° at a substrate temperature of 200°C. However, for even higher growth temperatures such as 300, 400, 500 and 600°C, the (002) peak positions were again observed to deviate from the angular value of powder peak but in the opposite direction, indicating change in the direction of stress as compared with unstressed MgZnO films [24].

The lattice constant for MgZnO films was evaluated from Vegard's law [25] and was used to calculate stress on MgZnO films grown on Si substrates [26].

$$c = 5.2042 - 0.072x, \tag{1}$$

$$a = 3.2491 + 0.047x, \tag{2}$$

$$\sigma = -4.5 \times 10^{12} \left(\frac{c - c_0}{c_0} \right). \tag{3}$$

The crystallite size (D) was calculated from the well-known Scherrer's formula [27]:

$$D = \frac{0.9\lambda}{A \cos \theta}, \tag{4}$$

where λ is the X-ray wavelength, A the full-width at half-maximum (FWHM) of the (002) diffraction peak and θ the Bragg diffraction angle of the (002) peak.

Numerical results demonstrated that MgZnO crystallite size was minimum with a value 41.6 nm at 300°C growth

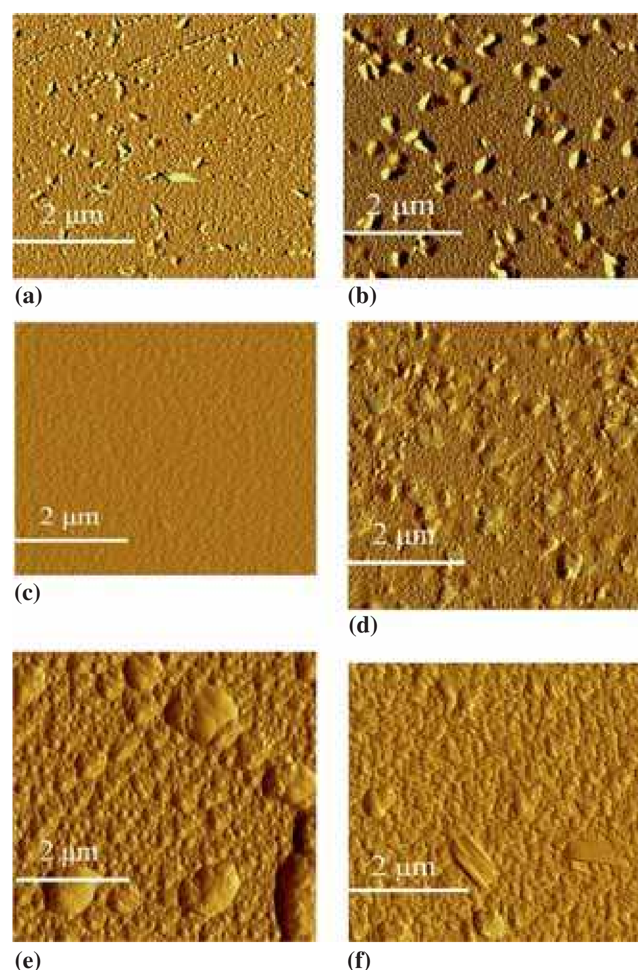

Figure 2. AFM images (5 μm × 5 μm scale) of MgZnO films deposited at the growth temperatures: (**a**) 100°C (**b**) 200°C (**c**) 300°C (**d**) 400°C (**e**) 500°C and (**f**) 600°C.

temperature and maximum with a value of 57.9 nm at 600°C growth temperature. Stress on films increased from -2.0486×10^{10} to 3.879×10^{10} dyne cm^{-2} as growth temperature increased from 100 to 600°C. The minimum stress value of -0.30641×10^{10} dyne cm^{-2} was achieved for MgZnO film grown at 200°C.

Table 1 shows the influence of growth temperature on stress and crystallite size of MgZnO thin films grown on the p-Si (001) substrate.

Atomic force microscopy (AFM) images shown in figure 2a–f illustrate the effect of growth temperature on surface morphology of MgZnO thin films. A maximum surface roughness of 70 Å on a 5 μm × 5 μm scale, was observed for the MgZnO film grown at 600°C. MgZnO film grown at 300°C was found to have minimum surface roughness of 17.5 Å.

Figure 3 describes the surface FE-SEM micrographs of the MgZnO films on Si substrates at temperature range 200, 400 and 600°C. MgZnO films were found to exhibit columnar, dense and hexagonal crystallites. The crystallite size and the morphology of film grown at 600°C showed larger and smooth surface.

The chemical states of zinc and magnesium elements was analysed by XPS. All XPS spectra were calibrated by the C 1s peak (284.6 eV) to compensate the charge effect. The addition of Mg to ZnO can either replace Zn^{2+} or form MgO secondary phase [28]. In the case of pure ZnO, the Zn $2p_{3/2}$ XPS peak appeared at 1022.03 eV represents the formation of Zn–O bonds while in case of MgZnO films, the Zn $2p_{3/2}$ peak shifted towards higher binding energies, which results from the replacement of Zn^{2+} by Mg^{2+} and an added Zn–O–Mg binding energy. Figure 4a shows XPS spectra of the O 1s core level in MgZnO films. The curve had been deconvoluted to generate three distinct and nearly Gaussian curves centred at binding energy levels of 529.6 eV (blue), 531 eV (green) and 531.8 eV (red). The oxygen (O 1s) spectra described the presence of both oxygen vacancies and interstitials in the film grown at 300°C. Oxygen interstitial defect concentration was found to be higher than vacancies since the intensity of 531.8 eV binding energy peak was larger than that at 529.6 eV.

Figure 4b shows the core level spectra of Mg $2p_{3/2}$ in MgZnO thin film. The Mg $2p_{3/2}$ XPS peak in the MgZnO thin film centred at around 49.6 eV can be ascribed to the presence of Mg^{2+} replacing Zn^{2+} [29]. No positive Mg $2p_{3/2}$ binding energy shift towards the Mg $2p_{3/2}$ (MgO) binding energy of around 50–51 eV was identified, which was in correlation with the absence of MgO phase.

Figure 4c illustrates the XPS spectra of Zn 2p levels in MgZnO thin films. The peaks of Zn $2p_{3/2}$ and Zn $2p_{1/2}$ spectra were appeared at binding energy values of 1022.03 and 1045.07 eV, respectively. This indicates the presence of the stable Zn–O bonds in ZnO crystal lattice structure. The binding energy difference between Zn $2p_{3/2}$ and Zn $2p_{1/2}$ was calculated to be 23.04 eV, which was characteristic value of ZnO [30–32].

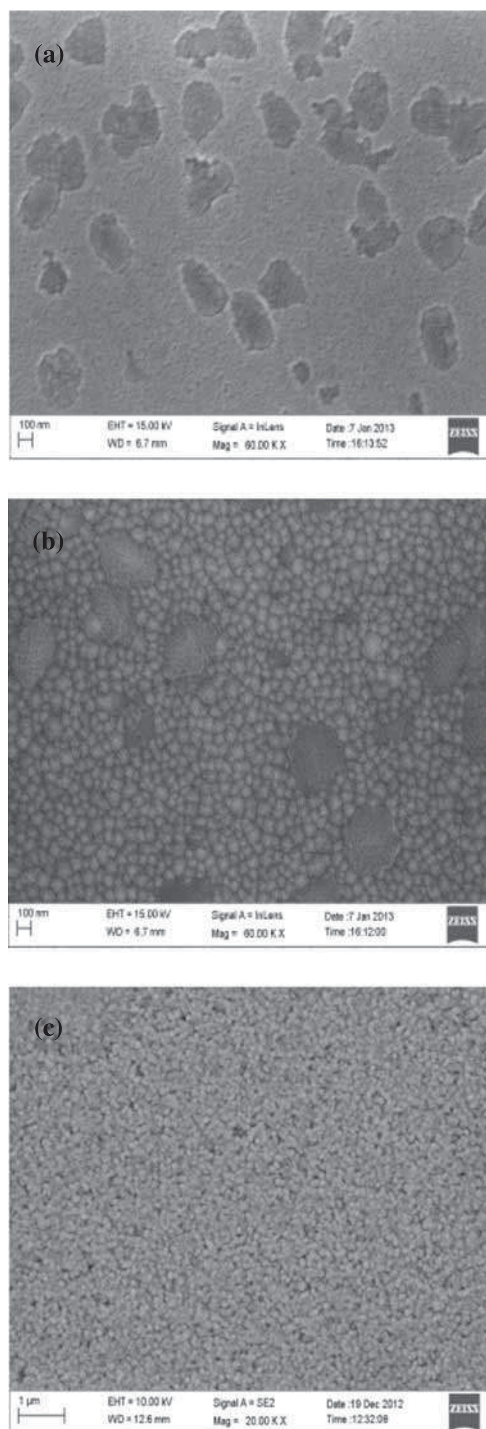

Figure 3. FE-SEM images of MgZnO samples grown on p-Si substrates at (**a**) 200°C (**b**) 400°C and (**c**) 600°C.

The variation of electrical properties of MgZnO films deposited at various substrate temperatures had been illustrated in figure 5. MgZnO films grown within the temperature range of 100–600°C showed n-type conductivity with high electron concentration of 10^{18} cm^{-3}, owing to the existence of native donor defects, such as O vacancies. MgZnO film, grown at 100°C, was found to have the highest carrier mobility of 40.25 cm^2 V^{-1} s^{-1} at room temperature with resistivity of

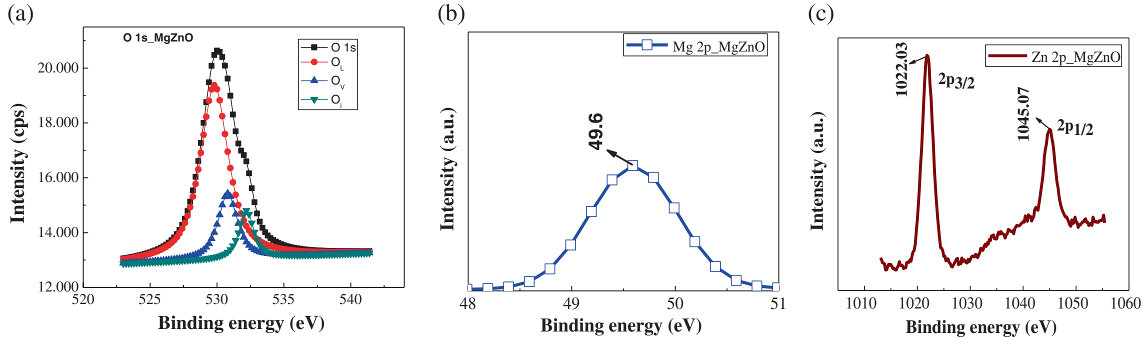

Figure 4. XPS spectra of (**a**) O 1s (O_i, O_L and O_V represented oxygen interstitials, lattice point and vacancies, respectively); (**b**) Mg 2p peak at 49.6 eV; and (**c**) Zn 2p having two sharp peaks at 1022.03 and 1045.07 eV in as-deposited MgZnO thin film grown at 300°C substrate temperature with Ar/O_2 ratio 2 : 4 at RF power = 65 W.

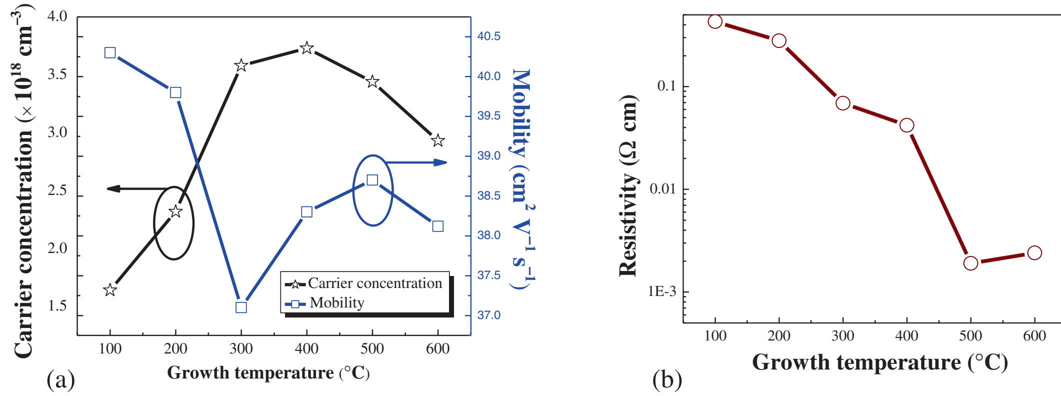

Figure 5. Variation of (**a**) carrier concentration and mobility and (**b**) resistivity of MgZnO thin films on Si at different substrate temperatures.

4.29×10^{-1} Ω cm and electron concentration of 1.53×10^{18} cm^{-3}. The free carrier mobility was almost 1.5 times higher than that obtained from MgZnO film grown by the other solid-state deposition techniques elsewhere [33,34]. It was observed that the structural properties of as-grown MgZnO thin films had a strong correlation with electrical properties. Calculated crystallite sizes of MgZnO grown at different substrate temperatures, as obtained from XRD measurements were observed to follow the same trend as carrier mobility values formulated by Hall measurement. At 300°C growth temperature, both carrier mobility and crystallite size were found to be minimum with values around 37 cm^2 V^{-1} s^{-1} and 41.67 nm, respectively. The possible explanation could be as when the crystallite size is small, the probability of having carriers to face more number of grain boundaries to move across the same distance along MgZnO surface and this might result in the reduction of carrier mobility.

I–V characteristics, as illustrated in figure 6, of MgZnO thin films under dark and under the influence of light illumination conditions were measured at room temperature, which is shown in figure 6. A non-linear behaviour in the semi-logarithmic I–V curves was observed in the MgZnO thin films in both dark and under light illumination. In case of light illumination, as there was an increase of the generation of electron–hole pairs in MgZnO films, non-ohmic behaviour was observed [35,36]. Due to the generation of more charge-carrying carriers, the value of current at a given bias voltage is larger in case of light illumination as compared with the corresponding value in dark conditions [35,36].

The photosensitivity of a semiconductor can be expressed as [37].

$$S = \frac{I_{\text{light}} - I_{\text{dark}}}{I_{\text{dark}}}. \quad (5)$$

The photosensitivity characteristics of the MgZnO films under different bias conditions are described in figure 7. MgZnO film grown at 100°C exhibited the highest photosensitivity of 1.62, when excited by the incident light. As observed from figure 7, the photosensitivity factor initially reduced somewhat as MgZnO growth temperature was increased up to 300°C, and then it improved marginally. This

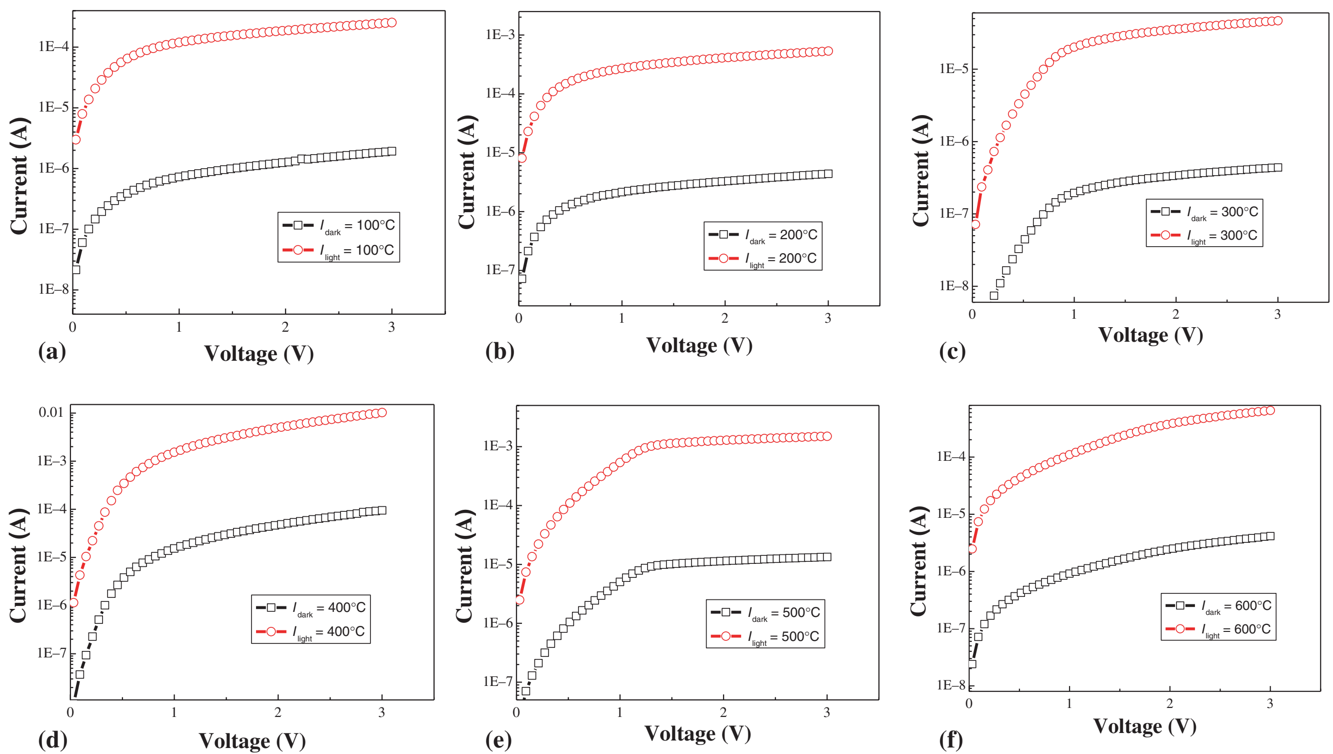

Figure 6. Semi-logarithmic ($I-V$) characteristics of MgZnO thin films (**a**) under dark condition and (**b**) under light illumination at temperatures: (**a**) 100, (**b**) 200, (**c**) 300, (**d**) 400, (**e**) 500 and (**f**) 600°C.

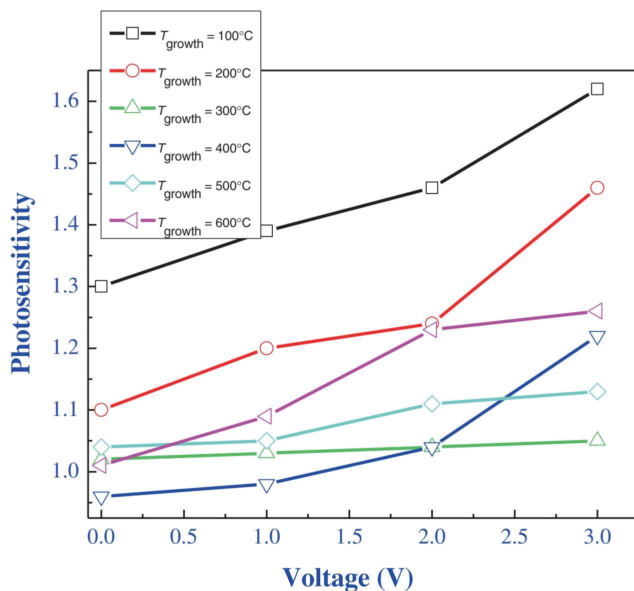

Figure 7. Photosensitivity factor w.r.t. voltage of MgZnO films.

behaviour was replicated by the carrier mobility variation with film growth temperature, as described in figure 5a. Compared with one of the best-reported values of photosensitivity factor from ZnO-material-based films available in the literature [38], ∼3.085-fold improved photosensitivity factor at the same bias voltage (2 V) was obtained. This actually confirmed superior growth quality of MgZnO films by DIBSD system. From the figure, it could be inferred that the grown MgZnO films are perfectly suitable for high-performance UV-detector and photosensor applications.

4. Conclusion

In summary, wurtzite $Mg_{0.1}Zn_{0.9}O$ thin films were deposited on the Si (001) substrate using DIBSD system and systematically studied to analyse the effect of growth temperature on structural, electrical and morphological properties of films. Smooth, high quality and preferred *c*-axis oriented MgZnO films can be synthesized by using $Mg_{0.1}Zn_{0.9}O$ target at RF power of 65 W with Ar/O_2 gas flow ratio of 2 : 4. The minimum stress value of -0.31×10^{10} dyne cm^{-2} was achieved for MgZnO film grown at 200°C. XPS studies confirmed the substitution of Zn^{2+} by Mg^{2+} in MgZnO thin films and the absence of MgO phase. At 300°C, both carrier mobility and crystallite size were found to be minimum with values around 37 cm^2 V^{-1} s^{-1} and 41.67 nm, respectively. MgZnO film, grown at 100°C, was observed to have the highest carrier mobility of 40.25 cm^2 V^{-1} s^{-1} at room temperature with a resistivity value of 4.29×10^{-1} Ω cm and electron concentration of 1.53×10^{18} cm^{-3}. Correlation between calculated crystallite size, as evaluated from XRD measurements and room-temperature carrier mobility, obtained from Hall measurements, was established for MgZnO, grown at different growth temperatures. A non-linear behaviour in the semi-logarithmic $I-V$ curves was observed in the MgZnO

thin films in both dark and under light illumination. MgZnO film grown at 100°C exhibited the highest photosensitivity of 1.62, when excited by the incident light. Compared with one of the best-reported values of photosensitivity factor from ZnO-material-based films, ∼3.085-fold improved photosensitivity factor at the same bias voltage (2 V) was obtained. From the measurement results, it could be inferred that the DIBSD-grown MgZnO films are perfectly suitable for high-performance UV-detector and photovoltaic applications.

Acknowledgements

This work was partially supported by Department of Science and Technology (DST) Fast Track Scheme for Young Scientist No. SR/FTP/ETA-101/2010. This work was also supported by DST Science and Engineering Research Board (SERB) project number SR/S3/EECE/0142/2011 and Council of Scientific and Industrial Research (CSIR) project number 22(0608)/12/EMR-II. We are also grateful for the Atomic Force Microscopy (AFM) Facility equipped at Sophisticated Instrument Centre (SIC), IIT Indore. We also express gratitude to Dr Mukul Gupta, UGC-DAE CSR, Indore, for XRD measurement of samples.

References

[1] Liao M and Koide Y 2006 *Appl. Phys. Lett.* **89** 113509

[2] Moon T H, Jeong M C, Lee W and Myoung J M 2005 *Appl. Surf. Sci.* **240** 280

[3] Look D C 2001 *Mater. Sci. Eng. B* **80** 383

[4] Polyakov A Y, Smirnov N B, Kozhukhova E A, Vdovin V I, Ip K, Heo Y W, Norton D P and Pearton S J 2003 *Appl. Phys. Lett.* **83** 1575

[5] Theodoropoulou N A, Hebard A F, Norton D P, Budai J D, Boatner L A, Lee J S, Khim Z G, Park Y D, Overberg M E, Pearton S J and Wilson R G 2003 *Solid-State Electron.* **47** 2231

[6] Kim H S, Pearton S J, Norton D P and Ren F 2008 *Appl. Phys. A* **91** 2

[7] Heo Y W, Tien L C, Norton D P, Kang B S, Ren F, Gila B P and Pearton S J 2004 *Appl. Phys. Lett.* **85** 2002

[8] Kwon Y, Li Y, Heo Y W, Jones M, Holloway P H, Norton D P, Park Z V and Li S 2004 *Appl. Phys. Lett.* **84** 2685

[9] Tuzemen S, Gur E, Yildirım T, Xiong G and Williams R T 2006 *J. Appl. Phys.* **100** 103513

[10] Studenikin S A, Golego N and Cocivera M 2000 *J. Appl. Phys.* **87** 2413

[11] Sharma P, Mansingh A and Sreenivas K 2002 *Appl. Phys. Lett.* **80** 553

[12] Yang W, Hullavarad S S, Nagaraj B, Takeuchi I, Sharma R P, Venkatesan T, Vispute R D and Shen H 2003 *Appl. Phys. Lett.* **82** 3424

[13] Ohtomo A, Kawasaki M, Koida T, Masubuchi K and Koinuma H 1998 *Appl. Phys. Lett.* **72** 2466

[14] Pandey S K, Pandey S K and Mukherjee S 2013 *Proceeding of the 5th IEEE international nanoelectronics conference* (INEC, Singapore)

[15] Liang M H, Ho Y T, Wang W L, Peng C Y and Li C 2008 *J. Cryst. Growth* **310** 1847

[16] Lu Y M, Wu C X, Wei Z P, Zhang Z Z, Zhao D X and Zhang J Y 2005 *J. Cryst. Growth* **278** 299

[17] Park W I, Yi G and Jang H M 2001 *Appl. Phys. Lett.* **79** 2022

[18] Liu W, Gu S L, Zhu S M, Ye J D, Qin F and Liu S M *et al* 2005 *J. Appl. Phys.* **277** 416

[19] Minemoto T, Negami T, Nishiwaki S, Takakura H and Hamakawa Y 2000 *Thin Solid Films* **372** 173

[20] Choi C H and Kim S H 2005 *J. Cryst. Growth* **283** 170

[21] Kar J P, Jeong M C, Lee W K and Myoung J M 2008 *Mater. Sci. Eng. B* **147** 74

[22] Pandey S K, Pandey S K, Mukherjee C, Mishra P, Gupta M, Barman S R, D'Souza S W and Mukherjee S 2013 *J. Mater. Sci.: Mater. Electron.* **24** 2541

[23] Pandey S K, Pandey S K, Deshpande U P, Awasthi V, Kumar A, Gupta M and Mukherjee S 2013 *Semicond. Sci. Technol.* **28** 085014

[24] American Standard for Testing of Materials—ASTM 36-1451

[25] Asharfi A B and Segawa Y 2005 *J. Vac. Sci. Technol. B* **23** 5

[26] Kumar R, Khare N, Kumar V and Bhalla G L 2008 *Appl. Surf. Sci.* **254** 20

[27] Cullity B D 1978 *Elements of X-ray diffraction* (Reading: Addison-Wesley) 2nd ed, p 102

[28] Park S M, Gu G H and Park C G 2011 *Phys. Status Solidi A* **208** 2688

[29] Lee C Y, Tseng T Y, Li S Y and Lin P 2006 *J. Appl. Phys.* **99** 024303

[30] Rao Kumar M C S, Safarulla A, Ganesan V, Barman S R and Sanjeeviraja C 2010 *Physica B* **405** 2226

[31] Islam M N, Ghosh T B, Chopra K L and Acharya H N 1996 *Thin Solid Films* **280** 20

[32] Fan H B, Yang S Y, Zhang P F, Wei H Y, Liu X L, Jiao C M, Zhu Q S, Chen Y H and Wang Z G 2007 *Chinese Phys. Lett.* **24** 2108

[33] Kim H S, Lugo F, Pearton S J and Norton D P 2008 *J. Vac. Sci. Technol. B* **26** 960

[34] Liu C Y, Xu H Y, Wang L, Li X H and Liu Y C 2009 *J. Appl. Phys.* **106** 073518

[35] Ilican S, Caglar Y and Caglar M 2008 *J. Optoelectron. Adv. Mater.* **10** 10

[36] Caglar Y, Caglar M, Ilican S and Ates A 2009 *J. Phys. D: Appl. Phys.* **42** 065421

[37] George P J, Sanchez-Juarez A and Nair P K 1996 *Semicond. Sci. Technol.* **11** 1090

[38] Zhou H, Fang G, Liu N and Zhao X 2011 *Nanoscale Res. Lett.* **6** 147